

# Measuring the Baryon Acoustic Oscillation scale using the SDSS and 2dFGRS

Will J. Percival<sup>1\*</sup>, Shaun Cole<sup>2</sup>, Daniel J. Eisenstein<sup>3</sup>, Robert C. Nichol<sup>1</sup>, John A. Peacock<sup>4</sup>, Adrian C. Pope<sup>5</sup>, Alexander S. Szalay<sup>6</sup>

<sup>1</sup> *Institute of Cosmology and Gravitation, University of Portsmouth, Portsmouth, PO1 2EG, UK*

<sup>2</sup> *Department of Physics, University of Durham, Science Laboratories, South Road, Durham DH1 3LE, UK*

<sup>3</sup> *Steward Observatory, University of Arizona, 933 N. Cherry Ave., Tucson, AZ 85121, USA*

<sup>4</sup> *SUPA; Institute for Astronomy, University of Edinburgh, Royal Observatory, Edinburgh EH9 3HJ, UK*

<sup>5</sup> *Institute for Astronomy, University of Hawaii, 2680 Woodlawn road, Honolulu, HI 96822, USA*

<sup>6</sup> *Department of Physics and Astronomy, The Johns Hopkins University, 3701 San Martin Drive, Baltimore, MD 21218, USA*

23 October 2018

## ABSTRACT

We introduce a method to constrain general cosmological models using Baryon Acoustic Oscillation (BAO) distance measurements from galaxy samples covering different redshift ranges, and apply this method to analyse samples drawn from the SDSS and 2dFGRS. BAO are detected in the clustering of the combined 2dFGRS and SDSS main galaxy samples, and measure the distance–redshift relation at  $z = 0.2$ . BAO in the clustering of the SDSS luminous red galaxies measure the distance–redshift relation at  $z = 0.35$ . The observed scale of the BAO calculated from these samples and from the combined sample are jointly analysed using estimates of the correlated errors, to constrain the form of the distance measure  $D_V(z) \equiv [(1+z)^2 D_A^2 cz/H(z)]^{1/3}$ . Here  $D_A$  is the angular diameter distance, and  $H(z)$  is the Hubble parameter. This gives  $r_s/D_V(0.2) = 0.1980 \pm 0.0058$  and  $r_s/D_V(0.35) = 0.1094 \pm 0.0033$  ( $1\sigma$  errors), with correlation coefficient of 0.39, where  $r_s$  is the comoving sound horizon scale at recombination. Matching the BAO to have the same measured scale at all redshifts then gives  $D_V(0.35)/D_V(0.2) = 1.812 \pm 0.060$ . The recovered ratio is roughly consistent with that predicted by the higher redshift SNLS supernovae data for  $\Lambda$ CDM cosmologies, but does require slightly stronger cosmological acceleration at low redshift. If we force the cosmological model to be flat with constant  $w$ , then we find  $\Omega_m = 0.249 \pm 0.018$  and  $w = -1.004 \pm 0.089$  after combining with the SNLS data, and including the WMAP measurement of the apparent acoustic horizon angle in the CMB.

**Key words:** cosmology: observations, distance scale, large-scale structure of Universe

## 1 INTRODUCTION

The physics governing the production of Baryon Acoustic Oscillations (BAO) in the matter power spectrum is well understood (Silk 1968; Peebles & Yu 1970; Sunyaev & Zel’dovich 1970; Bond & Efstathiou 1984, 1987; Holtzman 1989). These oscillatory features occur on relatively large scales, which are still predominantly in the linear regime; it is therefore expected that BAO should also be seen in the galaxy distribution (Meiksin et al. 1999; Springel et al. 2005; Seo & Eisenstein 2005; White 2005; Eisenstein et al. 2007). Consequently, BAO measured from galaxy surveys can be used as standard rulers to measure the geometry of the Universe through the distance–redshift relation (Blake & Glazebrook 2003; Seo & Eisenstein 2003).

BAO have now been convincingly detected at low redshift in

the 2dFGRS and SDSS galaxy samples (Cole et al. 2005; Eisenstein et al. 2005; Huetsi 2006). With the latest SDSS samples they are now detected with sufficient signal to use BAO alone to measure cosmological parameters (Percival et al. 2007a). This has emphasised the importance of accurate models for BAO in the galaxy power spectrum. On small scales, BAO will be damped due to non-linear structure formation (Eisenstein et al. 2007). Given the accuracy of current data, uncertainty in the exact form of this damping is not important, but it will become so for future data sets. On larger scales, there is currently no theoretical reason to expect systematic distortions greater than  $\sim 1\%$  in the BAO positions between the galaxies and the linear matter distribution (Seo & Eisenstein 2003; Springel et al. 2005; Seo & Eisenstein 2007; Angulo et al. 2007). Claims of  $> 1\%$  changes in the BAO position have used non-robust statistical measures of the BAO scale, such as the position of the bump in the correlation function, or peak locations in the power spectrum (Smith et al. 2007a,b; Crocce & Scoccimarro

\* E-mail: will.percival@port.ac.uk

2007). These are easily affected by smooth changes to the galaxy clustering amplitude as a function of scale. In this paper, we use a more robust approach: the BAO scale is defined via the locations where the BAO cross a smooth fit to the power spectrum.

Ideally we would use the BAO within two galaxy redshift surveys covering different narrow redshift slices to test a cosmological model using the following procedure:

- (i) Convert from galaxy redshift to distance assuming the cosmological model to be tested.
- (ii) Calculate the galaxy power spectra for the two samples.
- (iii) Measure the oscillations in each power spectrum around the known smooth underlying power spectrum shape.
- (iv) Test whether the change in scale between the two observed BAO positions agrees with that expected for this cosmological model.

Unfortunately, a number of complications prevent such a simple procedure from being used. In particular, this method requires a distance–redshift relation to be specified prior to measuring the BAO positions; but the errors and the effect of the survey selection function depend on this assumption, and these are computationally expensive to measure for many different models. In recent analyses (Percival et al. 2001; Cole et al. 2005; Tegmark et al. 2006), a fiducial cosmological model has been used to estimate the power spectrum, and the effect of this on the recovered shape of the power has been tested. However, when providing BAO distance scale measurements we need to allow for the change in the distance–redshift relation. In this paper, we calculate the power spectrum for a fiducial cosmology, and interpret these data as if the model cosmology had been analysed (incorrectly) assuming the fiducial model, therefore allowing for this effect. This procedure gives better noise properties for the derived parameters than recalculating the BAO for each model.

We test models against the data for general smooth forms of the distance–redshift relation, parametrised by a small number of nodes. This allows for surveys covering a range of redshifts, and has the advantage of allowing derived constraints to be applied to any model provided that it has such a smooth relation. Our “ideal” method also required us to know the power spectrum shape so we could extract the BAO. In this paper, we do not model this shape using linear CDM models. To immunise against effects such as scale-dependent bias, non-linear evolution, or extra physics such as massive neutrinos, we instead model the power spectrum shape by fitting with a cubic spline.

The method is demonstrated by analysing galaxy samples drawn from the combined SDSS and 2dFGRS (Section 5). Results are presented in Sections 5.3 & 7, and discussed in Section 8. This application is novel, as we combine the 2dFGRS and SDSS galaxy samples before calculating power spectra (the two data sets are introduced in Section 2). The blue selection in the 2dFGRS and the red selection in the SDSS galaxies emphasise different classes of galaxies with different large-scale biases – but these can be matched using a relative bias model leading to the same large-scale power spectrum amplitudes (Cole et al. 2005; Tegmark et al. 2006; Percival et al. 2007b). If there is scale-dependent bias, then the shape of the power spectrum calculated from the combined sample will be an average of the two individual power spectra, because we are selecting a mix of galaxy pairs. The exact mix will change with scales, but, this is not expected to be a significant concern for the BAO positions in the power spectra; these should be the same across all data sets, although there will be an effect on the damping of BAO on small scales (this is discussed in Section 3).

## 2 THE DATA

### 2.1 The SDSS data

The public SDSS samples used in this analysis are the same as described in Percival et al. (2007b). The SDSS (York et al. 2000; Adelman-McCarthy et al. 2006; Blanton et al. 2003; Fukugita et al. 1996; Gunn et al. 1998, 2006; Hogg et al. 2001; Ivezić et al. 2004; Pier et al. 2003; Smith et al. 2002; Stoughton et al. 2002; Tucker et al. 2006) Data Release 5 (DR5) galaxy sample is split into two subsamples: there are 465789 main galaxies (Strauss et al. 2002) selected to a limiting extinction-corrected magnitude  $r < 17.77$ , or  $r < 17.5$  in a small subset of the early data from the survey. In addition, we have a sample of 56491 Luminous Red Galaxies (LRGs; Eisenstein et al. 2001), which form an extension to the survey to higher redshifts  $0.3 < z < 0.5$ . Of the main galaxies, 21310 are also classified as LRGs, so our sample includes 77801 LRGs in total. Although the main galaxy sample contains significantly more galaxies than the LRG sample, the LRG sample covers more volume. The redshift distributions of these two samples are fitted as described in Percival et al. (2007b), and the angular mask is determined using a routine based on a HEALPIX (Górski et al. 2005) equal-area pixelization of the sphere (Percival et al. 2007b). In order to increase the volume covered at low redshift, we include the 2dFGRS sample, which for simplicity has been cut to exclude angular regions covered by the SDSS samples.

### 2.2 The 2dFGRS data

The full 2dF Galaxy Redshift Survey (2dFGRS) catalogue contains reliable redshifts for 221 414 galaxies selected to an extinction-corrected magnitude limit of approximately  $b_J = 19.45$  (Colless et al. 2001, 2003). For our analysis, we only select regions not covered by the SDSS survey, and we do not include the random fields, a set of 99 random 2 degree fields spread over the full southern galactic cap. This leaves 143 368 galaxies in total. The redshift distribution of the sample is analysed as in Cole et al. (2005), and we use the same synthetic catalogues to model the unclustered expected galaxy distribution within the reduced sample.

The average weighted galaxy densities in the SDSS and 2dFGRS catalogues were calculated separately, and the overall normalisation of the synthetic catalogues were matched to each catalogue separately using these numbers (see, for example, Cole et al. 2005 for details). The relative bias model described in Percival et al. (2007b) was applied to the SDSS galaxies and the bias model of Cole et al. (2005) was applied to the 2dFGRS galaxies. These normalise the large-scale fluctuations to the amplitude of  $L_*$  galaxies, where  $L_*$  is calculated separately for each survey. We therefore include an extra normalisation factor to the 2dFGRS galaxy bias model to correct the relative bias of  $L_*$  galaxies in the different surveys. This was calculated by matching the normalisation of the 2dFGRS and SDSS bias corrected power spectra for  $k < 0.1 h \text{ Mpc}^{-1}$ . 2dFGRS galaxies at a single location were all given the same expected bias, rather than having biases matched to their individual luminosities. This matches the method used for the SDSS, and makes the calculation of mock catalogues easier.

## 3 BAO IN THE GALAXY POWER SPECTRUM

In this section, we consider the relation between BAO measured from the galaxy distribution, and BAO in the linear matter distribution. We define the linear BAO as

$$B_{\text{lin}}(k) \equiv \frac{[T_{\text{full}}(k)]^2}{[T_{\text{no osc}}(k)]^2}, \quad (1)$$

which oscillates around  $B_{\text{lin}}(k) = 1$ .  $T_{\text{full}}(k)$  is the full linear transfer function, while  $T_{\text{no osc}}(k)$  is the same without the sinusoidal term arising from sound waves in the early universe. In the fitting formulae provided by Eisenstein & Hu (1998), this term is given by their equation 13, a modified sinc function. Note that  $T_{\text{no osc}}(k)$  contains the change in the overall shape of the power spectrum due to baryons affecting the small scale damping of perturbations, just not the oscillatory features.  $B_{\text{lin}}(k)$  can be considered as a multiplicative factor that corrects the smooth power spectrum to provide a full model.

Within the halo model (Seljak 2000; Peacock & Smith 2000; Cooray & Sheth 2002), the real-space galaxy power spectrum is related to the linear power spectrum by the addition of an extra smooth term, and multiplication by a smooth, possibly scale dependent, galaxy bias  $b(k)$

$$P_{\text{obs}}(k) = b^2(k)P(k)_{\text{lin}} + P(k)_{\text{extra}}. \quad (2)$$

The  $b^2(k)$  term can also be thought of as equivalent to the Q-model of Cole et al. (2005), used to model the transition between the linear matter power spectrum and observed galaxy power spectra. The form of Equation (2) matches that calculated by Scherrer & Weinberg (1998) from a general hierarchical clustering argument.  $b^2(k)$  and  $P(k)_{\text{extra}}$  are required to be slowly varying functions of  $k$  such that we can extract the BAO signal as follows. Substituting Equation (1) into Equation (2), and writing  $P_{\text{lin}}(k) = Ak^n [T_{\text{full}}(k)]^2$  gives

$$P_{\text{obs}}(k) = Ab^2(k)k^n B_{\text{lin}}(k) [T_{\text{no osc}}(k)]^2 + P(k)_{\text{extra}}. \quad (3)$$

We extract BAO from this observed power spectrum by dividing by a smooth model that, without loss of generality, we can choose to be

$$P(k)_{\text{smooth}} = Ab^2(k)k^n [T_{\text{no osc}}(k)]^2 + P(k)_{\text{extra}}, \quad (4)$$

so the oscillations in  $P_{\text{obs}}(k)/P(k)_{\text{smooth}}$  are

$$B_{\text{obs}}(k) = g(k)B_{\text{lin}}(k) + [1 - g(k)], \quad (5)$$

where

$$g(k) = \frac{Ab^2(k)k^n [T_{\text{no osc}}(k)]^2}{Ab^2(k)k^n [T_{\text{no osc}}(k)]^2 + P(k)_{\text{extra}}} \quad (6)$$

is smooth. The  $k$ -scales where  $B_{\text{obs}}(k) = 1$  occur where  $B_{\text{lin}}(k) = 1$ , showing that the oscillation wavelength is unchanged by the translation given by Equation (2). However, the positions of the maxima and minima will change as  $g(k)$  is expected to be asymmetric around the extrema. In fact, the detailed shape and amplitude of this damping term will depend on the cosmological model and on the properties of the galaxies being analysed. Eisenstein et al. (2007) have shown that  $g(k)$  can be approximated as a Gaussian convolution in position-space with  $\sigma_g = 10 h^{-1}$  Mpc for low redshift galaxies. For our default results presented in this paper, we fix the damping model to be Gaussian with  $\sigma_g = 10 h^{-1}$  Mpc, which is assumed not to change significantly over the redshifts or galaxy types used in the analysis. We consider variations in the BAO damping model in Section 6.2. Equation (5) shows that the observed power spectrum is constructed from a smooth component (Equation 4), and a multiplicative damped BAO model (Equation 5). We assume that such a decomposition can be performed for power spectra measured from galaxy samples drawn from the 2dFGRS and SDSS.

We model  $P(k)_{\text{smooth}}$  as a 9 node cubic spline (Press et al. 1992) designed to be able to match the overall shape of the power spectrum (i.e. to fit Equation 4), but not the BAO. The 9 nodes were fixed empirically at  $k = 0.001$ , and  $0.025 \leq k \leq 0.375$  with  $\Delta k = 0.05$ . A cubic spline  $\times$  BAO model with this node separation was found to be able to fit model linear power spectra by Percival et al. (2007a) and can match all of the power spectra presented in this paper without leaving significant residuals. The  $\chi^2$  values of the fits are all within the expected range of values. We also consider an offset node distribution in Section 6.2. The spline curve can be taken as the definition of ‘‘smooth’’: only effects that cannot be modelled by such a curve will affect the BAO positions. When fitting the observed BAO, we do not attempt to extract the BAO and then fit different models to these data, because the method by which the BAO are extracted might bias the result. Instead we fit combined cubic spline  $\times$  BAO models to the power spectra, allowing the spline fit to vary with each BAO model tested (this follows the method of Percival et al. 2007a).

We now consider how to model the BAO. Blake & Glazebrook (2003) suggest modelling  $B_{\text{lin}}(k)$  using a simple damped sinusoidal two-parameter function

$$B_{\text{lin}}(k) = 1 + Ak \exp \left[ - \left( \frac{k}{0.1 h \text{ Mpc}^{-1}} \right)^{1.4} \right] \sin \left( \frac{2\pi k}{k_A} \right), \quad (7)$$

where  $k_A = 2\pi/r_s$ , and  $r_s$  is the co-moving sound horizon scale at recombination at scale factor  $a_*$

$$r_s = \frac{1}{H_0 \Omega_m^{1/2}} \int_0^{a_*} \frac{c_S}{(a + a_{\text{eq}})^{1/2}} da. \quad (8)$$

Here, the amplitude  $A$  is treated as a free parameter. In this paper, we consider units  $h^{-1}$  Mpc, so working in these units  $H_0 \equiv 100$  in Equation (8). This simple function ignores issues such as the propagation of the acoustic waves after recombination. Although the sound speed drops radically at recombination, acoustic waves still propagate until the end of the ‘drag-epoch’. This leads to the slightly larger sound horizon as measured from the low- $z$  galaxy clustering data than the CMB. To include such effects, we use a BAO model extracted from a power spectrum calculated using the numerical Boltzmann code CAMB (Lewis et al. 2000), by fitting with a cubic spline  $\times$  BAO model. For simplicity, we index our results based on the sound horizon at recombination,  $r_s$ . In principle, there could be small errors here (i.e. the large-scale structure to CMB sound horizon ratio could be a function of cosmology), but the combination of the current results and WMAP data mean that we are not looking over that big a range of cosmological parameters. To test this, we have applied the spline  $\times$  BAO fit to CAMB power spectra for flat  $\Lambda$ CDM models with recombination sound horizon scales covering the 2- $\sigma$  range of our best fit numbers ( $\pm 6\%$ ). We find that the input sound horizon at recombination is recovered with less than 1% error from these fits, showing that this approximation is not important to current measurement precision.

For our default results, we extract the BAO model from a power spectrum calculated assuming  $\Omega_m = 0.25$ ,  $\Omega_b h^2 = 0.0223$  and  $h = 0.72$ . For these parameters  $r_s = 111.426 h^{-1}$  Mpc, calculated using formulae presented in Eisenstein & Hu (1998). Small differences of convention in computing the sound horizon scale can be accommodated by simply scaling to match this value for these cosmological parameters. If recovered bounds on  $r_s$  are to be used to constrain models where  $r_s$  is not calculated using the formulae presented in Eisenstein & Hu (1998), then our results should be shifted using the difference between  $r_s = 111.426 h^{-1}$  Mpc

and the model recombination sound horizon scale for  $\Omega_m = 0.25$ ,  $\Omega_b h^2 = 0.0223$  and  $h = 0.72$ .

## 4 OBSERVING THE BAO SCALE

### 4.1 Narrow redshift shell surveys

Suppose that a survey samples a narrow redshift shell of width  $\Delta z$  at redshift  $z$ . Furthermore, suppose that we are only interested in the clustering of galaxies pairs with small separations. For a given pair of galaxies,  $\Delta z$  and the angular separation  $\theta$  are fixed by observation, and we wish to measure the comoving separation for different cosmological models. In the radial direction, separations in comoving space scale with changes in the cosmological model as  $dr_c/dz \simeq \Delta r_c/\Delta z = c/H(z)$ , where  $r_c(z) \equiv \int c(1+z) dt$  is the comoving distance to a redshift  $z$ . In the angular direction, the comoving galaxy separation scales as  $\Delta r_c = \Delta\theta(1+z)D_A$ , where  $D_A$  is the standard angular diameter distance. Writing  $S_k \equiv (1+z)D_A$ ,

$$S_k(z) = \frac{c}{H_0} \begin{cases} |\Omega_k|^{-1/2} \sinh[\sqrt{\Omega_k} H_0 r_c(z)/c] & \text{if } (\Omega_k > 0), \\ H_0 r_c(z)/c & \text{if } (\Omega_k = 0), \\ |\Omega_k|^{-1/2} \sin[\sqrt{-\Omega_k} H_0 r_c(z)/c] & \text{if } (\Omega_k < 0). \end{cases} \quad (9)$$

where  $\Omega_k = 1 - \Omega_0$  and  $\Omega_0$  is the ratio of total to critical density today. If we assume that the pairs of galaxies are statistically isotropic, then we can combine the changes in scale and, to leading order, the measured galaxy separations scale with the cosmological model through the distance measure  $D_V(z) = [(1+z)^2 D_A^2 cz/H(z)]^{1/3}$ . Here, we have introduced a further factor of  $z$  to match the definition of  $D_V$  by Eisenstein et al. (2005): including functions of redshift does not change the dependence of  $D_V$  on different cosmological models. The position of features in the real space 2-pt functions, the (dimensionless) power spectrum and correlation function will approximately scale with this distance measure. It is worth emphasising that this is only an approximation, and would additionally be affected by redshift-space distortions and other anisotropic effects.

Following these approximations, for a survey covering a narrow redshift slice, the power spectrum  $P(k)$  only needs to be calculated for a single distance–redshift model. This is easiest if we assume a flat cosmological model so we can set up a comoving Euclidean grid of galaxies where BAO have the same expected scale in radial and angular directions. The power spectrum for other models can be recovered by simply rescaling the measured power in  $1/D_V(z)$ . Note that we could have instead worked in dimensionless units  $x/D_V(z)$ , where the power spectrum is independent of the comoving distance–redshift relation. The position of the BAO in the power spectrum constrain  $r_s/D_V(z)$ , which is analogous to the peak locations in the Cosmic Microwave Background (CMB) measuring  $r_s/S_k(z_{\text{ls}})$  (ignoring the astrophysical dependencies of the peak phases), where  $z_{\text{ls}}$  is the redshift of the last scattering surface.

### 4.2 Surveys covering a range of redshift

We now consider what it means to measure the BAO scale in surveys covering a range of redshifts. In this situation, the comoving distance–redshift model assumed in measuring  $\xi$  or  $P(k)$  becomes increasingly important. We first consider a simple survey covering two redshift shells, and then extrapolate to more general surveys.

Consider measuring the correlation function as an excess of

galaxy pairs in a survey covering two redshift shells at redshifts  $z_1$  and  $z_2$ . Our estimate of the correlation function from the combined sample will be the average of the correlation functions measured in the two redshift bins, weighted by the expected total number of pairs in each bin  $W(z_i)$ , and stretched by the distance  $D_V(z_i)$ . BAO in the power spectrum correspond to a “bump” in the correlation function, and the position of the bump scales with the BAO position, and therefore measures  $r_s/D_V(z_i)$ . For two redshift slices, the position of the bump in the combined correlation function depends on the average position of the bumps in the correlations functions for each slice, weighted by the total number of pairs in each bin. If  $D_V(z_1)$  is varied, then the same final BAO scale can be obtained from the combined data provided that  $D_V(z_2)$  is chosen such that  $[W(z_1)D_V(z_1) + W(z_2)D_V(z_2)]$  remains constant. Extending this analysis to a large number of redshift shells, we see that the measured BAO scale, assuming that this is measured from the mean position of the bump in the correlation function, depends on  $r_s/\hat{D}_V$  where

$$\hat{D}_V \equiv \int W(z)D_V(z) dz \quad (10)$$

Here, we do not have to worry about pairs of galaxies where the galaxies are in different shells because of the small separation assumption. The contributions from different redshifts  $W(z)$ , are calculated from the weighted galaxy redshift distribution squared. Because the weights applied to galaxies when analysing surveys tend to upweight low density regions the BAO will, in general, depend on a wider range of redshift than given by the radial distribution of galaxies.

Now suppose that an incorrect comoving distance–redshift model  $\bar{D}_V(z)$  was assumed in the measurement of  $\xi$  or  $P(k)$ . Furthermore, suppose that this model  $\bar{D}_V(z)$  has a different shape to the true  $D_V(z)$  but the same value of  $\hat{D}_V$ . In this situation, our measurement of  $r_s/\hat{D}_V$  is unbiased with respect to the true value. What has changed is that the BAO signal has been washed out: the recovered BAO in the power spectrum are of lower amplitude, and the peak in the correlation function broadens, because the BAO scales measured at different redshifts are not in phase, although they sum so that their average has the correct wave-scale. Note that if  $\bar{D}_V$  matches the true cosmological model, then there is no distortion of the BAO positions.

### 4.3 Fitting the distance–redshift relation

There are many different ways of parametrizing the distance–redshift relation. For example, we could consider a cubic spline fit to  $r_c(z)$ ,  $dr_c/dz$  or  $D_V(z)$ . For  $\Lambda$  cosmologies the comoving distance varies smoothly with redshift, and  $D_V(z)$ ,  $r_c(z)$  and  $dr_c/dz$  can all be accurately fitted by a spline with a small number of nodes. In this paper, we fit  $D_V(z)$  because of its physical meaning in a simplified survey analysis on small scales; but for non-flat cosmologies we cannot uniquely recover  $r_c(z)$  from  $D_V(z)$ . This is not a problem because we only expect to measure  $D_V(z)$ , and mocks calculated assuming the same  $D_V(z)$ , but with different geometries, should give the same cosmological constraints. Consequently, without loss of generality, we can assume flatness when calculating the comoving distances from  $D_V(z)$  in order to create mock catalogues, and use

$$r_c(z)^{\text{flat}} = \left[ 3 \int_0^z \frac{D_V^3(z')}{z'} dz' \right]^{1/3}. \quad (11)$$

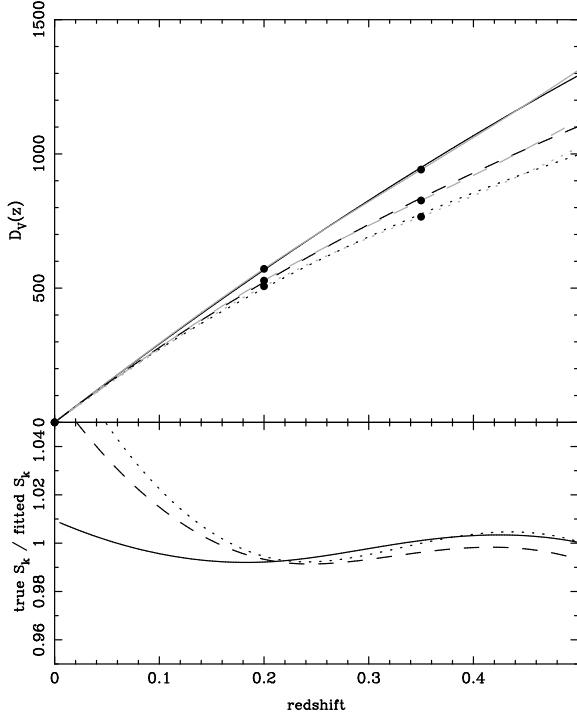


**Figure 1.** The result of fitting to  $D_V(z)$  using a cubic spline fit with three nodes at  $z = 0.0, 0.2, 0.35$  for  $0 < z < 0.5$ . We plot results for three cosmological models:  $\Lambda$ CDM ( $\Omega_m = 0.25$ ,  $\Omega_\Lambda = 0.75$ , solid lines), SCDM ( $\Omega_m = 1$ ,  $\Omega_\Lambda = 0$ , dotted lines), and OCDM ( $\Omega_m = 0.3$ ,  $\Omega_\Lambda = 0$ , dashed lines). The upper panel shows the true values of  $D_V(z)$  (black lines) compared with the spline fits (grey lines) with nodes (solid circles). The lower panel shows the resulting errors on  $S_k$  as given by Equation (9). For the redshift range  $z > 0.15$ , the error is  $< 1\%$ .

We now consider some of the practicalities of fitting the distance–redshift relation. Scaling of the distance–redshift relation can be mimicked by “stretching” the measured power spectra in  $k$ . Consequently, if we parametrize the distance–redshift model by  $N$  numbers, then power spectra only actually need to be calculated for a set of  $N - 1$  values. For example, if the distance–redshift model was parametrised by three nodes  $D_V(z_1)$ ,  $D_V(z_2)$  &  $D_V(z_3)$ , power spectra only need to be calculated for different  $D_V(z_2)/D_V(z_1)$  and  $D_V(z_3)/D_V(z_1)$  values. Working in units of  $h^{-1}$  Mpc and fitting  $dr_c/dz$ , is one way of including such a dilation of scale in the analysis: in these units the node at  $z = 0$  is fixed  $dr_c/dz|_{z=0} = c/H_0$ , and only  $N - 1$  nodes are free to vary. Allowing such a dilation at  $z = 0$ , may not be the optimal choice for the analysis of a survey at higher redshift.

By fitting the comoving distance (or a function of it), we hope to provide measurements that can be easily applied to any set of cosmological models, although we only have to analyse a small number of comoving distance–redshift relations. The cosmological models that can be tested require that the distance measure adopted can be well matched by the parametrisation used. In this paper, we model  $D_V(z)$  by a cubic spline fit with 2 nodes at  $z = 0.2$  and  $z = 0.35$ : consequently the results should only be used to delineate between cosmological models where  $D_V(z)$  is well modelled by such a fit. Fig. 1 shows fits of this form matched to a selection of standard cosmological models (assuming a constant weighted galaxy distribution with redshift). The error induced on the comoving distance as a result of fitting  $D_V(z)$  is small for these models.

The boundary conditions of the cubic spline are set so that the second derivatives are zero at  $z = 0$  and  $z = 0.35$ .

#### 4.4 Differential distance measurements

In order to break the degeneracy between distance measurements at different redshifts inherent in a single measurement of the BAO scale, we need to analyse the BAO position in multiple power spectra or correlation functions. This is true even if we are not in the regime where the small separation assumption holds, although the degeneracy would then be a more complicated function of the comoving distance than  $\hat{D}_V$  (Equation 10).

For the analysis of the 2dFGRS and SDSS DR5 galaxies presented in this paper, the sample is naturally split into main galaxies (2dFGRS and SDSS), SDSS LRGs, and the combination of the three samples. These samples obviously overlap in volume, so the derived power spectra will be correlated. However, using overlapping samples retains more information than contiguous samples which would remove pairs across sample boundaries. There is no double counting as each power spectrum contains new information, and correlations between different power spectra are included in the calculation of model likelihoods.

#### 4.5 Basic method

For each distance–redshift relation to be tested using the observed BAO locations, we could recalculate the power spectrum and measure the BAO positions. However, the likelihood of each model would not vary smoothly between different models because the shot noise term in each band–power varies in a complicated way with the distance–redshift relation. This would give a “noisy”, although unbiased, likelihood surface.

An alternative approach is to fix the distance–redshift relation used to calculate the power spectra. If this is different from the model to be tested, the difference can be accounted for by adjusting the window function - each measured data value has a different interpretation for each model tested. One advantage of such an approach is that the shot noise component of the data does not change with the model tested, leading to a smoother and easier to interpret likelihood surface. The primary difficulty is that the calculation of the window for each model is computationally intensive. We now consider the mathematics behind this approach.

Following Feldman et al. (1994), we define the weighted galaxy fluctuation field as

$$f(\mathbf{r}) \equiv \frac{1}{N} w(\mathbf{r}) [n_g(\mathbf{r}) - \alpha n_s(\mathbf{r})], \quad (12)$$

where  $n_g(\mathbf{r}) = \sum_j \delta(\mathbf{r} - \mathbf{r}_j)$  with  $\mathbf{r}_j$  being the location of the  $j$ th galaxy, and  $n_s(\mathbf{r})$  is defined similarly for the synthetic catalogue with no clustering. Here  $\alpha$  is a constant that matches the average densities of the two catalogues (see, for example, Percival et al. 2004), and  $N$  is a normalization constant defined by

$$N = \left\{ \int d^3r [\bar{n}(\mathbf{r}) w(\mathbf{r})]^2 \right\}^{1/2}. \quad (13)$$

$\bar{n}(\mathbf{r})$  is the mean galaxy density, and  $w(\mathbf{r})$  is the weight applied. The power spectrum of the weighted overdensity field  $f(\mathbf{r})$  is given by

$$\langle |F(\mathbf{k})|^2 \rangle = \int d^3r \int d^3r' \langle f(\mathbf{r}) f(\mathbf{r}') \rangle e^{i\mathbf{k} \cdot (\mathbf{r} - \mathbf{r}')}. \quad (14)$$

The important term when substituting Equation (12) into Equation (14) is the expected 2-point galaxy density given by

$$\langle n_g(\mathbf{r})n_g(\mathbf{r}') \rangle = \bar{n}(\mathbf{r})\bar{n}(\mathbf{r}') [1 + \xi(\hat{\mathbf{r}} - \hat{\mathbf{r}}')] + \bar{n}(\mathbf{r})\delta_D(\mathbf{r} - \mathbf{r}'). \quad (15)$$

If we analyse the galaxies using a different cosmological model to the “true” model, the 2-pt galaxy density depends on  $\hat{\mathbf{r}}$  and  $\hat{\mathbf{r}}'$ , the positions in the true cosmological model that are mapped to positions  $\mathbf{r}$  and  $\mathbf{r}'$  when the survey is analysed. Translating from the correlation function  $\xi(\hat{\mathbf{r}})$  to the power spectrum  $P(\hat{\mathbf{k}})$  in the true cosmological model gives

$$\xi(\hat{\mathbf{r}} - \hat{\mathbf{r}}') = \frac{1}{2\pi^2} \int P(\hat{\mathbf{k}}) e^{-i\mathbf{k} \cdot (\hat{\mathbf{r}} - \hat{\mathbf{r}}')} d^3\hat{\mathbf{k}}, \quad (16)$$

which can be substituted into Equation (15). Combining Equations (12 – 16) shows that the recovered power spectrum is a triple integral over the true power. If  $\hat{\mathbf{r}} = \mathbf{r}$ , this reduces to a convolution of the power spectrum with a “window function” (Feldman et al. 1994). If we now consider a piecewise continuous true power spectrum  $P(k) = \sum_i P_i[\Theta(k) - \Theta(k - k_i)]$ , where  $\Theta(k)$  is the Heaviside function, then the triple integral can be written as a linear sum over  $P_i$ ,  $\langle |F(\mathbf{k})|^2 \rangle = \sum_i W_i P_i$ . Because the radial interpretation changes between actual and measured clustering, spherically averaging the recovered power is no longer equivalent to convolving the power with the spherical average of the window function. Consequently, the window has to be estimated empirically from mock catalogues created with different true power spectra and analysed using a different cosmological model. The empirical window function can be calculated including both the change in cosmological model and the survey geometry.

## 5 ANALYSIS OF THE SDSS AND 2dFGRS

### 5.1 The observed BAO

Fig. 2 shows the BAO determined from power spectra calculated for the combined sample of SDSS main galaxies and 2dFGRS galaxies, the SDSS LRG sample, and the combination of these samples. The power spectra were calculated for  $N = 70$  band powers equally spaced in  $0.02 < k < 0.3 h \text{ Mpc}^{-1}$  using the method described in Percival et al. (2007a), assuming a flat  $\Lambda$  cosmology with  $\Omega_m = 0.25$ . Errors on these data were calculated from 2000 Log-Normal (LN) density fields (Coles & Jones 1991) covering the combined volume, from which overlapping mock samples were drawn with number density matched to each galaxy catalogue. The distribution of recovered power spectra includes the effects of cosmic variance and the LN distribution has been shown to be a good match to the counts in cells on the scales of interest  $> 10 h^{-1} \text{ Mpc}$  (Wild 2005), so these catalogues should also match the shot noise of the data. The catalogues do not include higher order correlations at the correct amplitude for non-linear structure formation, which are not included in the Log-Normal model. However, the BAO signal comes predominantly from large-scales that are expected to be in the linear or quasi-linear regimes, so these effects should be small. Each catalogue was calculated on a  $(512)^3$  grid covering a  $(4000 h^{-1} \text{ Mpc})^3$  cubic volume. The recovered power spectra from these mock catalogues were fitted with cubic spline  $\times$  BAO fits as described in Section 3, and the errors on the BAO were calculated after dividing by the smooth component of these fits.

We have fitted cubic spline  $\times$  BAO models to the SDSS and 2dFGRS power spectra using the method of Percival et al. (2007a). For each catalogue we have calculated the window function of the survey assuming a flat  $\Lambda$  cosmology with  $\Omega_m = 0.25$  (using the

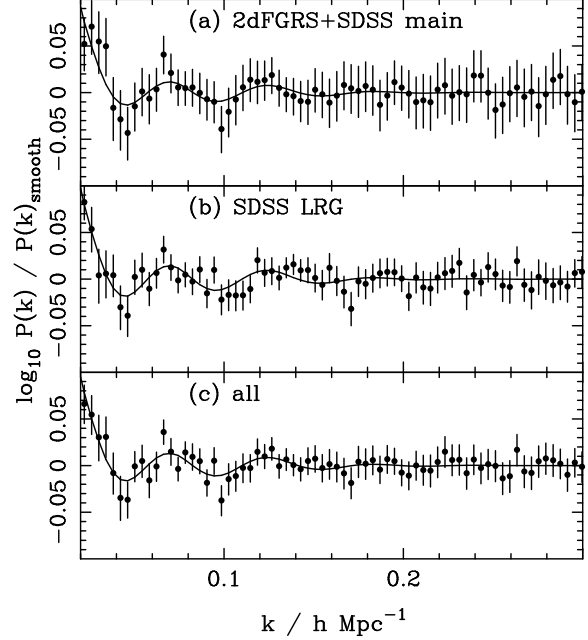


**Figure 2.** BAO in power spectra calculated from (a) the combined SDSS and 2dFGRS main galaxies, (b) the SDSS DR5 LRG sample, and (c) the combination of these two samples (solid symbols with  $1\sigma$  errors). The data are correlated and the errors are calculated from the diagonal terms in the covariance matrix. A Standard  $\Lambda$ CDM distance–redshift relation was assumed to calculate the power spectra with  $\Omega_m = 0.25$ ,  $\Omega_\Lambda = 0.75$ . The power spectra were then fitted with a cubic spline  $\times$  BAO model, assuming our fiducial BAO model calculated using CAMB, as described in Section (3). The BAO component of the fit is shown by the solid line in each panel.

method described in Percival et al. 2007a), and the covariance matrix from the LN catalogues, assuming that the power spectra band powers are distributed as a multi-variate Gaussian. The power spectrum for each sample was then fitted using cubic spline including or excluding the multiplicative BAO model calculated using CAMB as described in Section 3 for a flat  $\Lambda$  cosmology with  $\Omega_m = 0.25$ ,  $\Omega_b h^2 = 0.0223$  &  $h = 0.72$ . All three samples are significantly better fit by the models including BAO. For the combined data,  $-2\Delta \ln \mathcal{L} = 9.6$ , for the LRGs  $-2\Delta \ln \mathcal{L} = 7.4$ , and for the SDSS main + 2dFGRS galaxies  $-2\Delta \ln \mathcal{L} = 5.9$  for the likelihood ratios between best-fit model power spectra with BAO and without BAO.

Including the 2dFGRS data reduces the error on the derived cosmological parameters by approximately 25% for our combined analysis of three power spectra. The BAO calculated from just the SDSS main galaxies and the combination of the SDSS main galaxies and the LRGs are shown in Fig. 3. From just the SDSS main galaxies,  $-2\Delta \ln \mathcal{L} = 4.5$  for the likelihood ratios between best-fit model power spectra with BAO and without BAO. There is no change in the significance of the BAO detection from the combined SDSS LRG and main galaxy sample from including the 2dFGRS galaxies.

The power spectra plotted in Fig. 2 are clearly not independent. Some of the deviations between model and data in the combined catalogue can be traced back to similar distortions in either the main galaxy or LRG power spectra. The LRGs have a greater weight when measuring the clustering of the combined sample on large-scales compared with the lower redshift galaxies, while the low redshift galaxies have a stronger weight when measuring the clustering on smaller scales. The combined sample includes addi-

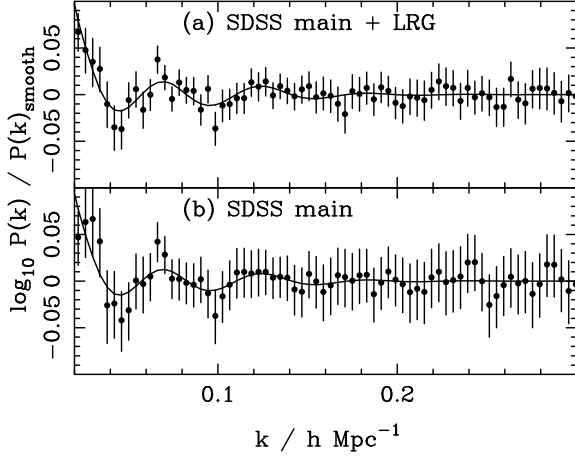


**Figure 3.** As Fig. 2, but for power spectra calculated from (a) the combined SDSS DR5 LRG and main galaxy sample, (b) the SDSS main galaxy sample.

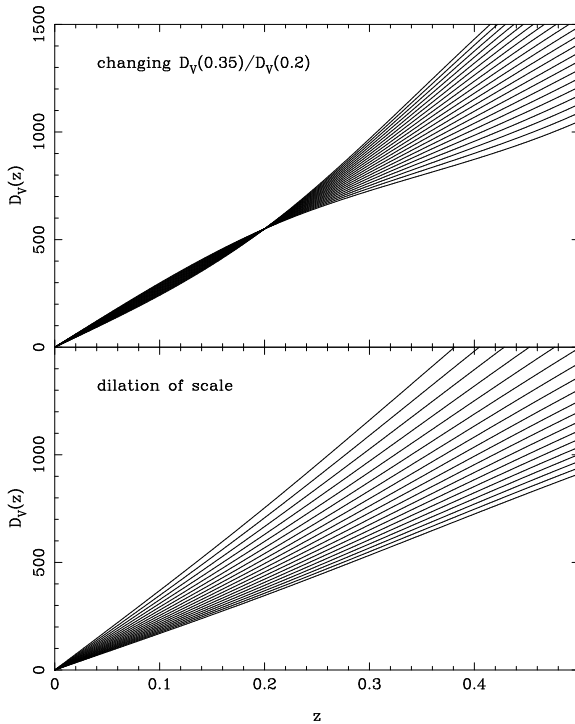


**Figure 4.** Two possible ways of changing the distance–redshift model tested against the data. Dilating the scale can be achieved by simply scaling the measured power spectra and windows, while changing the form of the distance–redshift relation requires recalculation of the windows.

tional galaxy pairs where the galaxies lie in different subsamples. All three samples also cover different redshift ranges. As discussed in Section 4 this means that they all contain unique cosmological information. By simultaneously analysing all three power spectra, allowing for the fact that they may be correlated, we can therefore extract more cosmological information than by analysing a single power spectrum.

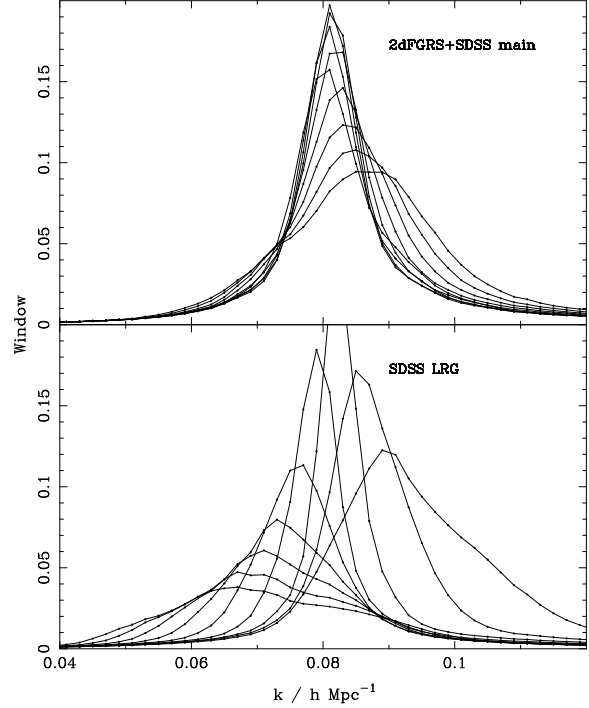


**Figure 5.** The window function linking the input power spectrum with an observed band-power at  $k = 0.08 h \text{ Mpc}^{-1}$  (calculated assuming a  $\Lambda$ CDM model), for the SDSS LRG and 2dFGRS + SDSS main galaxy catalogues. Window functions are plotted for 9 distance–redshift models with  $D_V(0.2) = 550 h^{-1} \text{ Mpc}$  and  $800 < D_V(0.35) < 1200 h^{-1} \text{ Mpc}$ . For the LRGs, the peak  $k$ -value of the power that contributes to this measured band-power decreases with increasing  $D_V(0.35)$ .

## 5.2 Fitting the distance–redshift relation

We test distance–redshift models that are given by a cubic spline fit to  $D_V$ , with one node fixed at  $D_V(0.2) = 550 h^{-1} \text{ Mpc}$  and 41 equally separated values of another node at  $D_V(0.35)$  with  $800 < D_V(0.35) < 1200 h^{-1} \text{ Mpc}$ .  $D_V(0) = 0$  is assumed for each model. These models are shown in the top panel of Fig. 4. We also allow the distances to be scaled, which is shown in the lower panel of Fig. 4 for fixed  $D_V(0.35)/D_V(0.2)$ . This scaling can be accomplished without recalculation of the power spectra, windows or covariances, which can all be scaled to match the new distance–redshift relation. In the spline  $\times$  BAO model that we fit to the data, we allow the spline nodes to vary with this scaling, so that the spline nodes always match the same locations in the power spectra.

Fig. 2 shows that we can detect BAO in three catalogues: SDSS LRG, SDSS main + 2dFGRS and combined SDSS + 2dFGRS. We now provide some of the practical details of how we constrain the fit to  $D_V(z)$  using these data. For each model value of  $D_V(0.35)/D_V(0.2)$ , the measured power spectra are a convolution of the true power, based on the survey geometry and the difference between the model cosmology and the cosmology used to calculate the power. In order to calculate the window function for each convolution, we have calculated 10000 Gaussian random fields, allowing the phases and input power spectra to vary. We assume that the true power is piecewise continuous in bins of width  $0.002 h \text{ Mpc}^{-1}$  between  $0 < k < 0.4 h \text{ Mpc}^{-1}$ . We calculated 50 fields where power was only added in one of these 200 bins. Each field was calculated on a  $(512)^3$  grid covering a  $(4000 h^{-1} \text{ Mpc})^3$  cubic volume. Each Gaussian random field was

then translated onto a grid assuming a distance–redshift relation following the fiducial  $\Lambda$ CDM cosmology, and is then sampled and weighted to match the actual survey. The average recovered power spectrum from each set of 50 realisations then gives part of the window function of the data given each model, and combining data for all 200 bins allows the full window function to be estimated. Fig. 5 shows a few of the resulting window functions for the recovered band-power at  $k = 0.08 h \text{ Mpc}^{-1}$ . These models were calculated with  $D_V(0.2) = 550 h^{-1} \text{ Mpc}$  and 9 values of  $D_V(0.35)$  with  $800 < D_V(0.35) < 1200 h^{-1} \text{ Mpc}$  with separation  $50 h^{-1} \text{ Mpc}$ . These numerically determined window functions include both the effects of the volume covered by the survey, and the different distance–redshift relation. For the LRGs, when we analyse the data assuming a  $\Lambda$ CDM cosmology, if the true value of  $D_V(0.35)$  increases, the scales contributing to a given band-power also increase, and the peak value in the window function in  $k$ -space decreases. The corresponding window functions for the lower redshift data plotted in the upper panel of Fig. 5 do not show such a significant change because the node at  $D_V(0.2)$  remains fixed.

We calculate the expected covariances from the LN catalogues described in Section 5.1. These catalogues were calculated allowing for overlap between samples, and power spectra were calculated as for the actual data. Covariances (internal to each  $P(k)$  and between different power spectra) were recovered assuming that the power spectra are distributed as a multi-variate Gaussian. For the set of models tested, we do not change the covariance matrix with  $D_V(0.35)/D_V(0.2)$  (the change in models shown in the top panel of Fig. 4), because the recovered data power spectra do not change when altering this parameter combination. Consequently, in this direction, it is the correlations between data points that primarily change. Tests with different matrices show that this has a negligible effect across the set of models, but recalculating the covariance matrices for each model introduces significant noise into the likelihood surfaces. We do scale the covariance matrix with the data when we dilate in scale (the change in models shown in the bottom panel of Fig. 4).

### 5.3 Results

In this section, we present likelihood surfaces calculated by fitting models to the BAO detected in power spectra from the different samples. In order to remove small likelihood differences caused by different fits to the overall shape of the power spectrum, we subtract the likelihood of the best-fit model without BAO from each likelihood before plotting. The likelihood differences between models with no BAO is caused by the effect of the different window functions on allowed shapes of the spline part of the model.

Fig. 6 presents likelihood surfaces calculated by fitting cubic spline  $\times$  BAO models to power spectra calculated from different sets of data. The upper row of panels show likelihoods plotted as a function of the 2 parameters used in the analysis,  $D_V(0.35)/D_V(0.2)$ , and  $r_s/D_V(0.2)$  which is used to parametrise the dilation of scale. The lower panels show the same likelihood surfaces after a change of variables to  $r_s/D_V(0.2)$  and  $r_s/D_V(0.35)$ . BAO within the SDSS main galaxy and 2dFGRS power spectrum primarily fix the distance to the  $z = 0.2$ , while the LRG power spectrum measures the distance to  $z = 0.35$ . When we jointly analyse the power spectra from the low redshift data, the LRGs and the combination of these samples, we find  $r_s/D_V(0.2) = 0.1980 \pm 0.0058$  and  $r_s/D_V(0.35) = 0.1094 \pm 0.0033$  (unless stated otherwise all errors given in this paper are  $1-\sigma$ ). These constraints are correlated with correlation coefficient

of 0.39. The likelihood surface is well approximated by treating these parameters as having a multi-variate Gaussian distribution with these errors (the left panel of Fig. 7 shows this approximation compared with the true contours). For completeness, the method for likelihood calculation is described in Appendix A.

For our conventions,  $r_s = 111.426 h^{-1} \text{ Mpc}$  for  $\Omega_m = 0.25$ ,  $\Omega_b h^2 = 0.0223$  and  $h = 0.72$ . Hence, if  $\Omega_m h^2 = 0.13$  and  $\Omega_b h^2 = 0.0223$ , we find  $D_V(0.2) = 564 \pm 23 h^{-1} \text{ Mpc}$  and  $D_V(0.35) = 1019 \pm 42 h^{-1} \text{ Mpc}$ ; one can scale to other values of  $\Omega_m h^2$  and  $\Omega_b h^2$  using the sound horizon scale formula from Equation (8).

Without the 2dFGRS data, the low-redshift result reduces to  $r_s/D_V(0.2) = 0.1982 \pm 0.0067$ , while the  $z = 0.35$  result is unchanged: as expected, the 2dFGRS data primarily help to limit the distance–redshift relation at  $z \sim 0.2$ . We can ratio the high and low redshift BAO position measurements to remove the dependence on the sound horizon scale  $r_s$ . From all of the data, we find  $D_V(0.35)/D_V(0.2) = 1.812 \pm 0.060$ . This is higher than the flat  $\Lambda$ CDM value, which for  $\Omega_m = 0.25$  and  $\Omega_\Lambda = 0.75$  is  $D_V(0.35)/D_V(0.2) = 1.66$ .

## 6 TESTING THE METHOD

### 6.1 The range of scales fitted

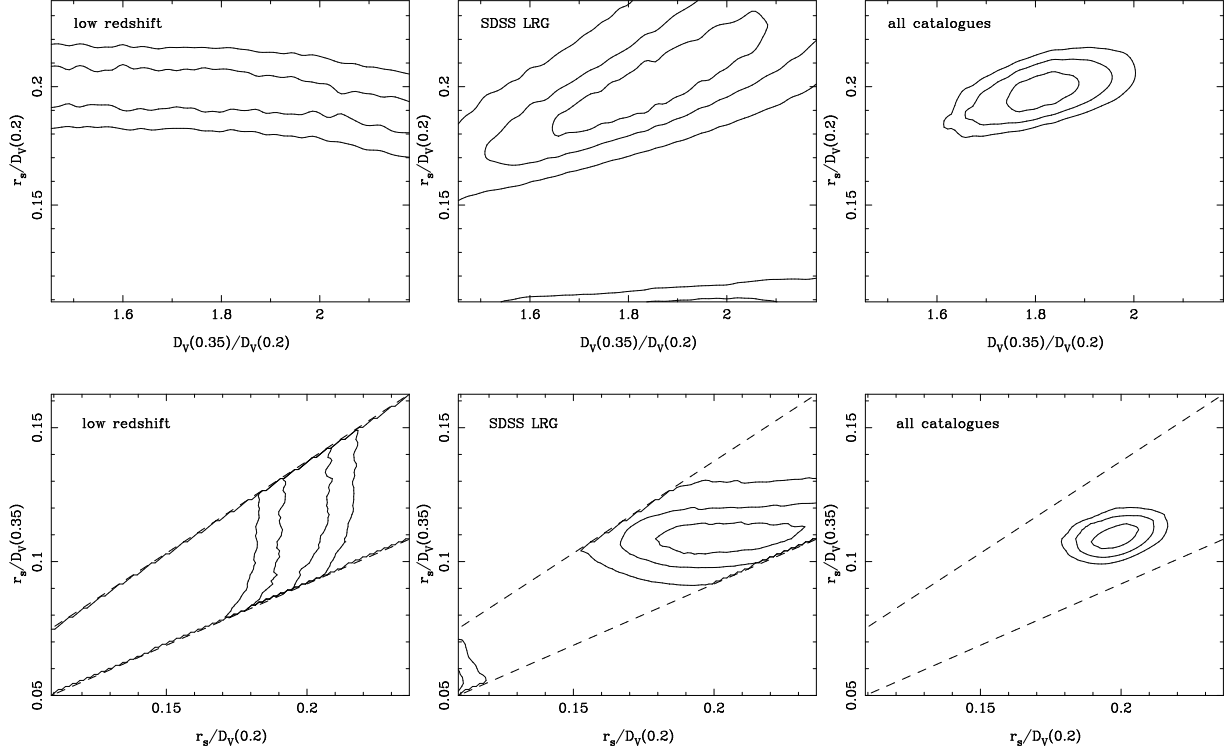
Fig. 7 shows the effect of changing the range of  $k$ -values fitted on the likelihood surface. Reducing the upper limit from  $k = 0.3 h \text{ Mpc}^{-1}$  to  $k = 0.2 h \text{ Mpc}^{-1}$  does not change the significance of the best fit, compared to the no-BAO solution. However, this reduction in the range of  $k$  values fitted increases the possibility of the BAO model fitting spurious noise because the  $0.2 < k < 0.3 h \text{ Mpc}^{-1}$  data provide a long lever arm to fix the overall power spectrum shape. Increasing the lower  $k$  limit considered in the fit from  $k = 0.02 h \text{ Mpc}^{-1}$  to  $k = 0.05 h \text{ Mpc}^{-1}$  does reduce the significance of the BAO detection, because the BAO signal is strongest on large scales. However, there is only a small offset in the position of the likelihood maximum if we do this, and the recovered ratio  $D_V(0.35)/D_V(0.2)$  is unchanged. This gives us confidence that we are picking up the oscillatory BAO signal, and that the large scale features of the BAO, which depend on the details of the BAO production, do not contribute significantly to the fit.

### 6.2 The spline $\times$ BAO model

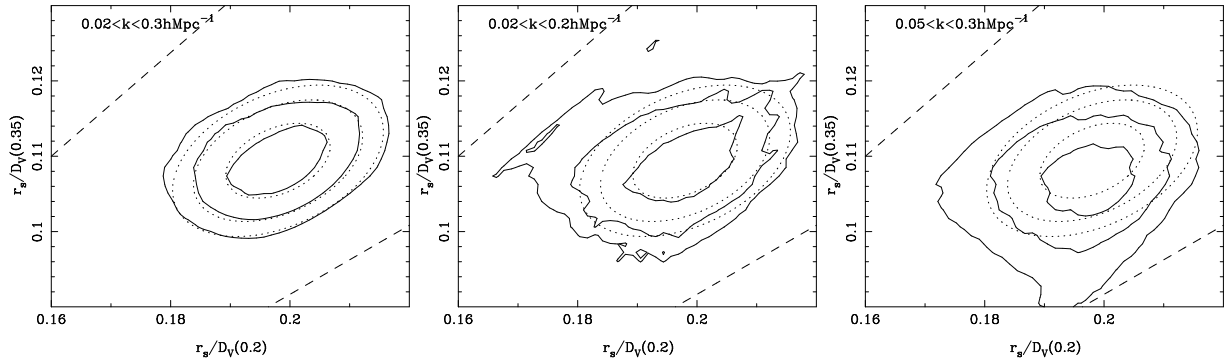
Fig. 8 shows likelihood surfaces calculated by fitting the measured power spectra with different spline  $\times$  BAO models. We have considered offsetting the nodes of the spline curve to  $k = 0.001 h \text{ Mpc}^{-1}$  and 8 nodes with  $0.05 \leq k \leq 0.4 h \text{ Mpc}^{-1}$  and separation  $\Delta k = 0.05 h \text{ Mpc}^{-1}$ . Using this form for the spline curve alters the best-fit parameters to  $r_s/D_V(0.2) = 0.1956 \pm 0.0068$  and  $r_s/D_V(0.35) = 0.1092 \pm 0.0039$ . This spline fit is a better match to the BAO signal on scales  $k < 0.1 h \text{ Mpc}^{-1}$ , leading to a smaller difference between likelihoods for spline  $\times$  BAO models and models with just a spline curve, and larger errors on the recovered parameters.

Fig. 8 shows that there is a small systematic change in the distance ratio  $D_V(0.35)/D_V(0.2)$  when the amplitude of the BAO damping is altered. Increasing the width of the Gaussian damping model to  $\sigma_g = 20 h^{-1} \text{ Mpc}$  for the BAO fitted to the three power spectra decreases the best-fit ratio to  $D_V(0.35)/D_V(0.2) =$





**Figure 6.** From left to right: Likelihood surfaces calculated from fitting a cubic spline  $\times$  BAO model to a single power spectrum calculated from the combined main SDSS galaxy + 2dFGRS sample, to a single power spectrum calculated using for SDSS LRG sample, and to both these power spectra and the additional power spectrum calculated from the combined catalogue. Where more than one power spectrum is fitted, we allow for correlated errors between the power spectra. Likelihood contours were plotted for  $-2 \ln \mathcal{L} = 2.3, 6.0, 9.2$ , corresponding to two-parameter confidence of 68%, 95% and 99% for a Gaussian distribution. In the upper row, we plot the contours as a function of  $r_s/D_V(0.2)$ , calculated by dilating the scales of the power spectra, windows and covariances, and  $D_V(0.35)/D_V(0.2)$ , for which different windows were calculated. These likelihoods are plotted as a function of  $r_s/D_V(0.2)$  and  $r_s/D_V(0.35)$  in the lower row of this figure. Here the dashed lines show the limits of the parameter space tested.



**Figure 7.** Likelihood surfaces as plotted in Fig. 6, but now fitting to different ranges in  $k$ -space (solid contours). As a reference, the dotted contours show the Gaussian approximation to the  $0.02 < k < 0.3 h \text{Mpc}^{-1}$  likelihood surface which has  $r_s/D_V(0.2) = 0.1980 \pm 0.0058$  and  $r_s/D_V(0.35) = 0.1094 \pm 0.0033$ , and correlation coefficient of 0.39. Dashed lines show the limit of the parameter ranges considered as shown in Fig. 6.

$1.769 \pm 0.079$ . Removing the small-scale BAO damping for all models increases the ratio to  $D_V(0.35)/D_V(0.2) = 1.858 \pm 0.051$ . When changing the damping term, the best fit value of  $r_s/D_V(0.2)$  does not change significantly, and the change in the ratio comes almost entirely from different fitted values of  $r_s/D_V(0.35)$ , which is most strongly limited by the LRG power spectrum. To help to explain this effect, Fig. 9 shows BAO models with different values of  $D_V(0.35)/D_V(0.2)$  and damping strength, compared with the observed LRG BAO. The BAO observed in the LRG power spectrum occur on larger

scales than predicted by our fiducial  $\Lambda$ CDM model, where  $D_V(0.35)/D_V(0.2) = 1.66$ . By increasing the strength of the damping, we reduce the significance of the small-scale signal leading to increased errors and a ( $< 1\sigma$ ) systematic shift to smaller  $D_V(0.35)/D_V(0.2)$ .

If we include  $\sigma_g$  as a fitted parameter with a uniform prior, allowing  $\sigma_g$  to vary between power spectra, we obtain best-fit values  $\sigma_g = 7.3 \pm 4.3 h^{-1} \text{Mpc}$  for the low redshift data,  $\sigma_g = 1.4 \pm 2.2 h^{-1} \text{Mpc}$  for the LRGs, and  $\sigma_g = 4.7 \pm 2.6 h^{-1} \text{Mpc}$  for the power spectrum of the combined sample.

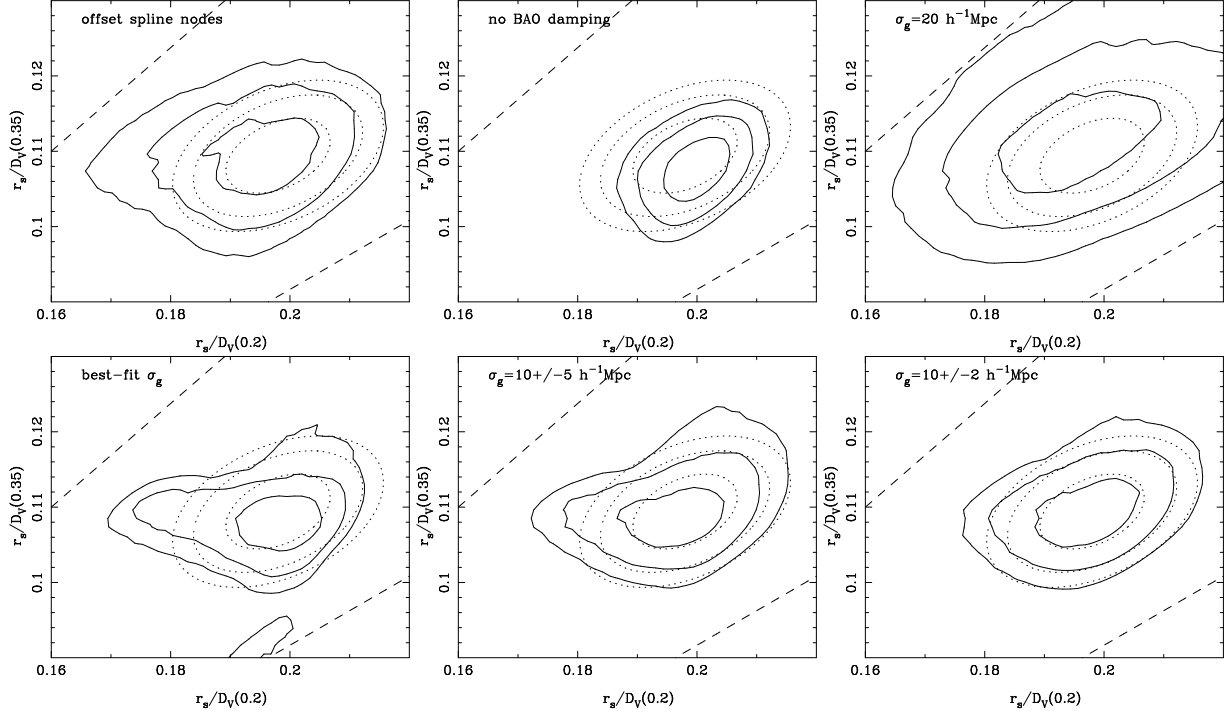


**Figure 8.** Likelihood surfaces as plotted in Fig. 6, but now calculated fitting the measured power spectra with different spline  $\times$  BAO models (solid contours). Other lines are as in Fig. 7. Top row, from left to right: we consider a spline curve with nodes  $k = 0.001 h \text{ Mpc}^{-1}$  and  $k = 0.05 + n0.05 h \text{ Mpc}^{-1}$  with  $n = 1, 2, \dots, 7$ , which are offset in  $k$  compared with our default separation. We use our default spline fit, but remove the small-scale BAO damping. We use the default spline fit, but increase the position-space BAO damping to be a Gaussian with  $\sigma_g = 20 h^{-1} \text{ Mpc}$ . Bottom row: likelihood surface calculated allowing the damping term, parametrised by  $\sigma_g$ , to float with a uniform prior, and with Gaussian priors  $\sigma_g = 10 \pm 5 h^{-1} \text{ Mpc}$  or  $\sigma_g = 10 \pm 2 h^{-1} \text{ Mpc}$ .

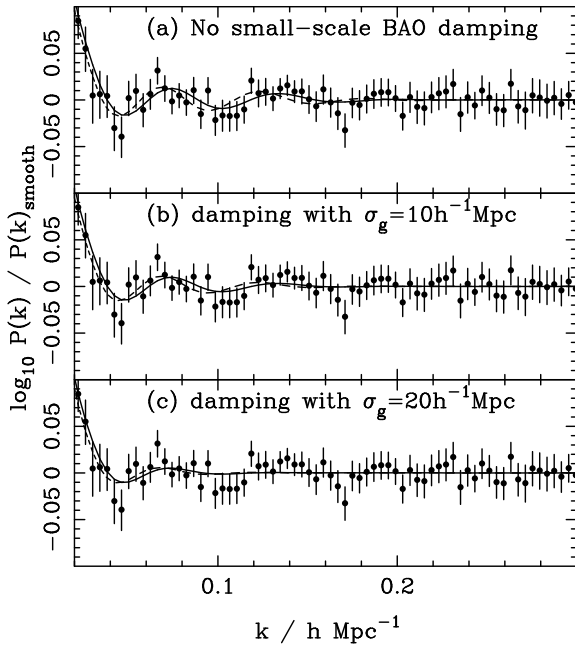


**Figure 9.** As Fig. 2, but only for the LRG power spectrum, plotted against BAO models with different levels of small-scale BAO damping (a) no damping, (b)  $\sigma_g = 10 h^{-1} \text{ Mpc}$ , (c)  $\sigma_g = 20 h^{-1} \text{ Mpc}$ . The solid line is for  $D_V(0.35)/D_V(0.2) = 1.82$ , while the dashed line is calculated for  $D_V(0.35)/D_V(0.2) = 1.66$ .  $D_V(0.2) = 568$ , matching the values of our fiducial  $\Lambda\text{CDM}$  model.

Here  $D_V(0.35)/D_V(0.2) = 1.827 \pm 0.061$ . However, the inclusion of these extra parameters increases the noise in the likelihood surfaces. This likelihood surface is shown in Fig. 8, revealing a spur at constant  $r_s/D_V(0.35)$  following models with extreme damping of the low redshift data, weakening the constraint on  $r_s/D_V(0.2)$ . The extra minima at  $r_s/D_V(0.35) < 0.1$  is due to models with strongly damped BAO fitted to both the low redshift and combined power spectra. Likelihood surfaces calculated assuming that  $\sigma_g$  has a Gaussian prior with  $\sigma_g = 10 \pm 5 h^{-1} \text{ Mpc}$  or  $\sigma_g = 10 \pm 2 h^{-1} \text{ Mpc}$  are also plotted in Fig. 8. As expected, there is a smooth transition between these likelihood surfaces, and allowing a small error in  $\sigma_g$  does not change the likelihood significantly from the fixed  $\sigma_g = 10 h^{-1} \text{ Mpc}$  form.

We have also considered how using approximations to the BAO model affects the fits. Fig. 10 shows the likelihood of different  $r_s/D_V(0.2)$  and  $r_s/D_V(0.35)$  values, with BAO models calculated using the Eisenstein & Hu (1998) fitting formulae, and the simple model of Blake & Glazebrook (2003), as given by Equation (7). The BAO models have been damped assuming  $\sigma_g = 10 h^{-1} \text{ Mpc}$  for a Gaussian position-space convolution as described in Section 3. For the Eisenstein & Hu (1998) fitting formulae, we have considered two approaches to calculating the likelihood: either using a fiducial BAO model (calculated for the same cosmological parameters as our standard CAMB model) and stretching this model in amplitude and scale, or allowing  $\Omega_m$  to vary to match the desired comoving sound horizon scale, and allowing  $\Omega_b/\Omega_m$  to fix the BAO amplitude. The second approach allows the BAO model on scales  $k < 0.05 h \text{ Mpc}^{-1}$  to change with cosmological parameters for fixed value of  $D_V(0.2)$ . Ideally, in order to accurately model the BAO on large scales we should

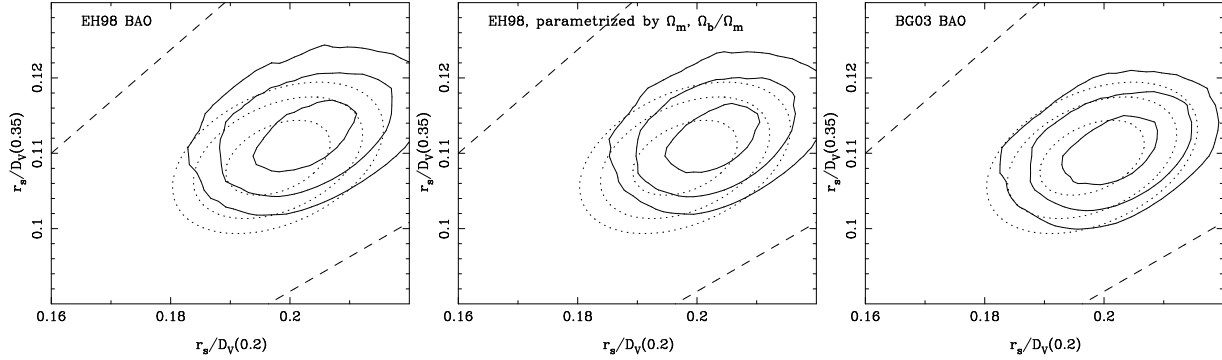


**Figure 10.** Likelihood surfaces as plotted in Fig. 6, but now calculated using different BAO models (solid contours). Other lines are as in Fig. 7. From left to right: we use the transfer function fits of Eisenstein & Hu (1998) to model the BAO, calculated for our fiducial cosmology and stretched in amplitude and scale as for the standard CAMB model. We again use the fits of Eisenstein & Hu (1998) but now allow  $\Omega_m$  to change to fix the sound horizon scale, and marginalise over the amplitude parametrised by  $\Omega_b/\Omega_m$ . We model the BAO using the simple model of Equation (7).

separate  $r_s$  and the distance scale in the fits. However, there is little change in the recovered parameters between these two approaches, demonstrating that this level of complexity is not required for current data precision. There is a change in the recovered parameters of order  $< 1\sigma$ , with best-fit parameters for the Eisenstein & Hu (1998) fits  $r_s/D_V(0.2) = 0.2020 \pm 0.0060$  and  $r_s/D_V(0.35) = 0.1120 \pm 0.0033$  with correlation coefficient of 0.41. For the Blake & Glazebrook (2003) fits,  $r_s/D_V(0.2) = 0.2011 \pm 0.0058$  and  $r_s/D_V(0.35) = 0.1104 \pm 0.0034$  with correlation coefficient of 0.37. The definition of  $r_s$  is built into the Blake & Glazebrook (2003) fit, and will have a different fiducial value to the other fits.

We might expect the ratio  $D_V(0.35)/D_V(0.2)$  to be more robust to changes in the BAO model as it measures the relative positions of the BAO at the different redshifts. In essence, by considering this ratio, we are testing how well the BAO from low and high redshift match. Our standard CAMB fit gave  $D_V(0.35)/D_V(0.2) = 1.812 \pm 0.060$ . Using the Eisenstein & Hu (1998) BAO fitting formulae gives  $D_V(0.35)/D_V(0.2) = 1.800 \pm 0.066$ , while using the Blake & Glazebrook (2003) fit gives  $D_V(0.35)/D_V(0.2) = 1.827 \pm 0.061$ . These are all consistent at  $1\sigma$ .

## 7 COSMOLOGICAL CONSTRAINTS

We consider three ways of using the BAO scale measurements to restrict cosmological models. Using just the observed position of the BAO in the power spectra analysed, we can measure  $D_V(0.35)/D_V(0.2)$ . Alternatively, we can compare these distance scales with the apparent acoustic horizon angle in the CMB: The WMAP experiment has measured this as  $\theta_A = 0.5952 \pm 0.0021^\circ$  (Spergel et al. 2007). For simplicity, we ignore the 0.4% error on this measurement, which is negligible compared with the large-scale structure distance errors, and assume that  $r_s/S_k(1098) = 0.0104$ . Including this measurement to remove the dependence on  $r_s$  gives  $S_k(1098)/D_V(0.2) = 19.04 \pm 0.58$  and  $S_k(1098)/D_V(0.35) = 10.52 \pm 0.32$ . The third possibility is that we model the co-moving sound horizon scale, and simply use the derived bounds on  $r_s/D_V(0.2)$  and  $r_s/D_V(0.35)$ . This relies on fitting the comoving sound horizon scale at recombination in addition to the distance–redshift relation, and has additional parameter dependencies on  $\Omega_m h^2$  and  $\Omega_b h^2$ . In order to calculate  $r_s$  for each cosmological model tested, we assume that  $\Omega_b h^2 = 0.0223$  and  $\Omega_m h^2 = 0.1277$ , matching the best-fit WMAP numbers for

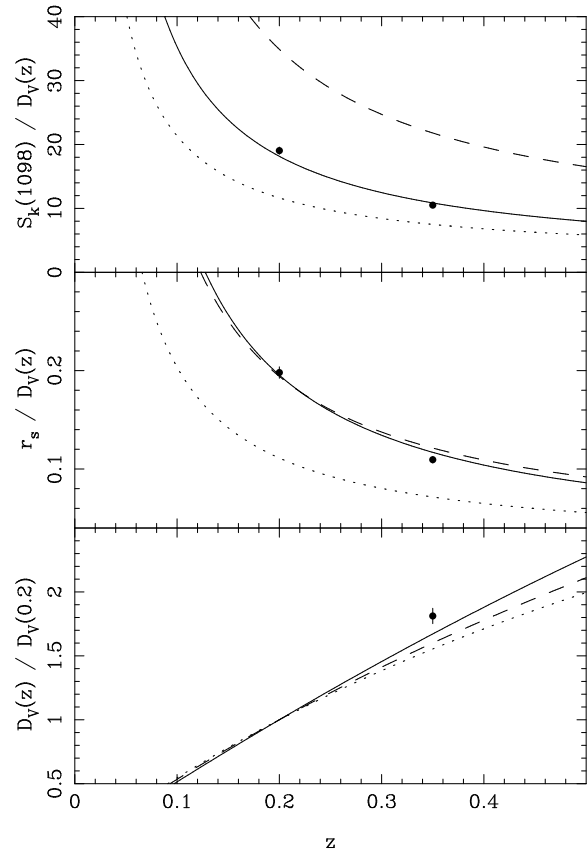


**Figure 11.** Three different ways of using BAO to test cosmological models. The panels from top to bottom show the constraints on  $S_k(1098)/D_V(z)$ ,  $r_s/D_V$ , and  $D_V(z)/D_V(0.2)$  (solid circles with  $1\sigma$  errors). For many of the data points the errors are smaller than the symbols. These data are compared with three cosmological models:  $\Lambda$ CDM ( $\Omega_m = 0.25$ ,  $\Omega_\Lambda = 0.75$ , solid lines), SCDM ( $\Omega_m = 1$ ,  $\Omega_\Lambda = 0$ , dotted lines), and OCDM ( $\Omega_m = 0.3$ ,  $\Omega_\Lambda = 0$ , dashed lines), as plotted in Fig. 1. In order to calculate  $r_s$  and hence  $r_s/D_V$ , we used the fitting formulae of Eisenstein & Hu (1998), assuming  $\Omega_b h^2 = 0.0223$  and  $\Omega_m h^2 = 0.1277$ , matching the best-fit WMAP numbers for  $\Lambda$ CDM cosmologies (Spergel et al. 2007). Although the best-fit  $D_V(0.35)/D_V(0.2)$  appears to be further from the  $\Lambda$ CDM model than in the other panels, this is just a consequence of  $r_s/D_V(0.2)$  being greater than and  $r_s/D_V(0.35)$  being less than the  $\Lambda$ CDM model.

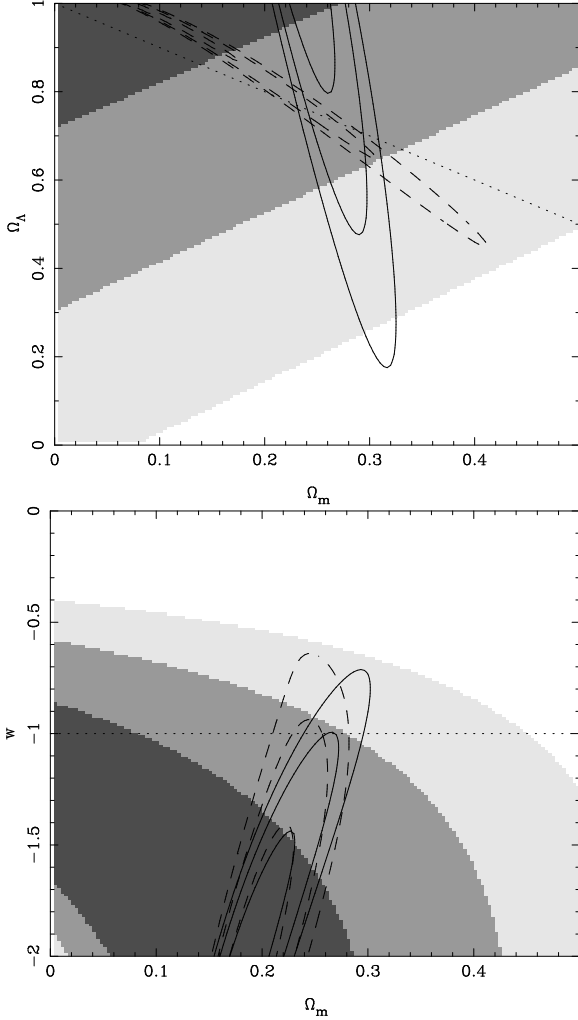


**Figure 12.** Top panel: Likelihood surfaces assuming a  $\Lambda$ CDM model parametrised by  $\Omega_m$  and  $\Omega_\Lambda$ . Contours and delineations between shaded regions are plotted for  $-2\ln\mathcal{L} = 2.3, 6.0, 9.2$ . The shaded regions show the likelihood given just  $D_V(0.35)/D_V(0.2)$ . The solid contours were calculated by modelling  $r_s$  and using constraints on  $r_s/D_V(0.2)$  and  $r_s/D_V(0.35)$ , and the dashed contours by including the CMB peak position measurement, and use  $S_k(1098)/D_V(0.2)$  and  $S_k(1098)/D_V(0.35)$ . The dotted line shows the locus of flat models. Bottom panel: likelihood contours calculated using the same data, but now for flat cosmological models with constant dark energy equation of state parameter  $w$ . Here the dotted line shows  $w = -1$ .

$\Lambda$ CDM cosmologies (Spergel et al. 2007). We do not include errors on these parameters, so our recovered errors from fitting  $r_s/D_V$  will be underestimated. The distance ratios  $D_V(0.35)/D_V(0.2)$  and  $S_k(1098)/D_V$  are independent of  $h$  and  $\Omega_b$ . These three possible ways of using the large-scale structure data are shown in Fig. 11, where we compare to three cosmological models.

We demonstrate the consistency of the BAO measurements by considering how they restrict two sets of cosmological models. The top panel of Fig. 12 shows likelihood contours for standard  $\Lambda$ CDM cosmologies, parametrised by  $\Omega_m$  and  $\Omega_\Lambda$ . The three ways of using the large-scale structure data that we have considered constrain different parameter combinations, and the location of their peak likelihoods do not coincide, although their 95% confidence intervals do overlap. In the lower panel we consider flat models with a constant dark energy equation of state parameter  $w$  that is allowed

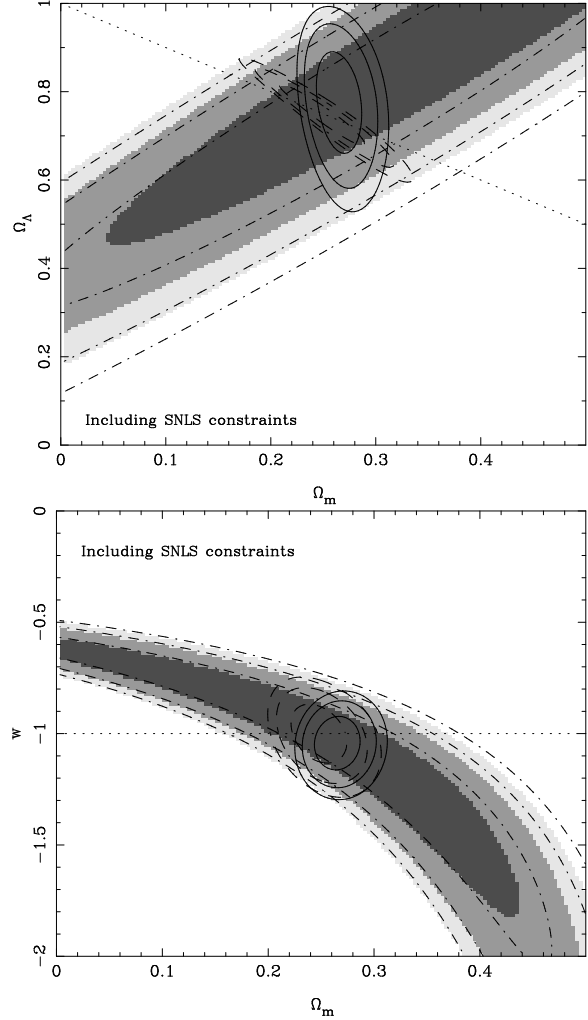


**Figure 13.** As Fig. 12, but now additionally using the SNIa data presented in Astier et al. (2006) in the Likelihood calculation. The shaded region, dashed and solid contours were calculated using the BAO based measurements described in the caption to Fig. 12. The dot-dashed contours show the likelihood surface calculated from just the SNLS data.

to vary from  $w = -1$ . Here,  $w < -1$  is favoured at a significance of  $1.4\sigma$ , from the  $D_V$  ratio assuming a flat prior on  $\Omega_m$ .

In Fig. 13 we have included constraints from the set of supernovae given in Astier et al. (2006). The tightest bounds on models are obtained if we include the ratio of the sound horizon scale at recombination to the angular diameter distance to last scattering calculated from CMB data, which then give a likelihood degeneracy that is approximately orthogonal to the supernovae likelihood degeneracy. Including the CMB data gives  $\Omega_m = 0.252 \pm 0.027$  and  $\Omega_\Lambda = 0.743 \pm 0.047$  for  $\Lambda$ CDM models. The curvature is found to be  $\Omega_k = -0.004 \pm 0.022$ . For flat models, with constant equation of state parameter  $w$ , we find  $\Omega_m = 0.249 \pm 0.018$  and  $w = -1.004 \pm 0.089$ .

## 8 DISCUSSION

We have introduced a general method for providing constraints on the distance–redshift relation using BAO measured from galaxy power spectra. The method can be applied to different galaxy sur-

veys, or to subsamples drawn from a single survey that cover different redshift ranges. At the heart of the method is a likelihood calculation, matching data and model power spectra, assuming that these have a multi-variate Gaussian distribution. We now review the components required for this calculation:

**PARAMETERS** The distance–redshift relation is parametrized using a spline fit in  $D_V(z)$  with a small number of nodes,  $D_V(z_i)$ . We can simply scale measured power spectra to follow a multiplicative shift of all  $D_V(z_i)$ , so we take as parameters  $D_V(z_i)/D_V(z_j)$ ,  $i \neq j$ , and  $D_V(z_1)$  (this was discussed in Section 4). This parametrization allows the results to be used to constrain general cosmological models that have such a smooth  $D_V(z)$ , without having to specify the set of models before the start of the analysis.

**DATA** The galaxies are split into subsamples covering different (possibly overlapping) redshift ranges. The power spectra for these samples are calculated assuming a fiducial cosmological model (Section 4). The position of the BAO in each power spectrum depends on a weighted integral of the distance–redshift relation for the range of redshifts covered by the sample from which the power spectrum is calculated. Consequently, by fitting power spectra from different samples, we can measure the ratio of distances to different redshifts.

**BAO MODEL** BAO are extracted from a model power spectrum calculated using CAMB, by fitting with a spline  $\times$  BAO model, as fitted to the observed galaxy power spectra. These BAO are stretched to allow for varying  $r_s/D_V(z_1)$  (Section 5.1).

**MODEL** The model is formed from a smooth spline curve multiplied by the BAO model (Section 5.1). This is convolved with the window function, which corrects for both the survey geometry, and the difference between the fiducial cosmology (at which the data power spectra were calculated), and the cosmological model to be tested (Section 4.5). The window functions were calculated using realisations of Gaussian random fields.

**ERRORS** Covariance matrices for the power spectra were calculated from Log-Normal realisations of galaxy distributions. Covariances between the different power spectra of different galaxy samples were included.

**NUISANCE PARAMETERS** The spline nodes giving the shapes of the power spectra were fixed at their best fit values for each model tested. We are therefore left with a likelihood measurements for a set of  $r_s/D_V(z_1)$  and  $D_V(z_i)/D_V(z_j)$ ,  $i \neq j$  values.

This analysis method has been used to jointly analyse samples of galaxies drawn from the SDSS and 2dFGRS. BAO were calculated by fitting a fiducial power spectrum calculated by CAMB (Lewis et al. 2000). We have considered using fitting formulae to calculate the BAO (Eisenstein & Hu 1998; Blake & Glazebrook 2003), and find changes in the recovered BAO scale of order  $1\sigma$ . Such a dependence was also found recently by Angulo et al. 2007 when fitting simulated data, and it is clear that the combined 2dFGRS+SDSS data now reveal the BAO with sufficient accuracy that we need to take care when modelling the BAO.

The BAO scale measurements were used to set limits on two sets of cosmological models: Standard  $\Lambda$  models, and flat models with constant dark energy equation of state. When we analyse flat  $\Lambda$ CDM models, we find similar errors on the matter density to those obtained by Percival et al. (2007a), where these models were directly compared with the data. The SNIa data from Astier et al. (2006) provide cosmological constraints that have a similar degeneracy direction to the lower redshift BAO constraint on  $D_V(0.35)/D_V(0.2)$ . However, if we include the information from the position of the peak in the WMAP CMB data, or model the

sound horizon scale at recombination then the likelihoods become complementary. These two approaches provide different best-fit parameters, although they are consistent at the  $1\sigma$  level. For  $\Lambda$ CDM models  $\Omega_m = 0.266 \pm 0.015$  if we model the sound horizon scale, or  $\Omega_m = 0.252 \pm 0.027$  including the CMB data. Similarly, for flat models with constant  $w$ , we find  $w = -1.045 \pm 0.080$  if we model the sound horizon scale, or  $w = -1.004 \pm 0.088$  including the CMB data.

For flat models with constant  $w$ , the differential distance measurement  $D_V(0.35)/D_V(0.2)$  favours  $w < -1$ . However, it is worth noting that Fig. 12 shows that the total density ( $\Omega_{\text{tot}}$ ) and  $w$  are highly coupled, so allowing curvature to vary would significantly weaken this conclusion (Clarkson et al. 2007). The SNLS supernovae data favour  $w \simeq -1$ , hinting at a discrepancy between low and high redshift. Fitting to the SNLS SNIa data gives  $D_V(0.35)/D_V(0.2) = 1.666 \pm 0.010$  for the set of  $\Lambda$ CDM models considered, or  $D_V(0.35)/D_V(0.2) = 1.665 \pm 0.010$  for flat models with constant dark energy equation of state.

The tests presented in Section 6.2 show that the measured distance ratio from the current BAO data is sensitive to the damping model. This is clear from Fig. 9, where it is apparent that there is a small offset between all models and the positions of the first and second peaks in the LRG BAO. By increasing the BAO damping, we decrease the significance of the second peak compared with the first, and change the fitted ratio  $D_V(0.35)/D_V(0.2)$ . However, our default choice of the damping model – a Gaussian convolution in position space with  $\sigma_g \sim 10 h^{-1} \text{Mpc}$  – is well motivated by current simulation results (Eisenstein et al. 2007; Angulo et al. 2007). This gives  $D_V(0.35)/D_V(0.2) = 1.812 \pm 0.060$ , which is offset by  $2.4\sigma$  from the SNIa results. If this is not a case of extreme bad luck, we must therefore consider at least one of the following options:

- (i) The damping model needs to be revised and made more sophisticated;
- (ii) The data/analysis is flawed in a way that evades the tests we have performed so far;
- (iii) The simple  $\Lambda$  model is wrong.

For the Gold supernovae data set (Riess et al. 2004), the significance of any evidence for  $w < -1$  at low redshift would increase because this SNIa dataset also favours strong dark energy at  $z < 0.3$  – so it is conceivable that this discrepancy could be genuinely cosmological in origin. However, in this paper we only compare with the SNLS data because of the benefits of considering homogeneous data. It will be interesting to recalculate this significance when the SDSS supernova survey (Nichol 2007) is complete, as it focuses on  $z < 0.5$ , and should either confirm or reject any deviations from a simple  $\Lambda$ CDM model at these low redshifts.

## ACKNOWLEDGEMENTS

WJP is grateful for support from a PPARC advanced fellowship. WJP acknowledges useful conversations with Sanjeev Sehra, and constructive comments from David Weinberg on an early draft of this manuscript. Simulated catalogues were calculated and analysed using the COSMOS Altix 3700 supercomputer, a UK-CCC facility supported by HEFCE and PPARC in cooperation with CGI/Intel.

The 2dF Galaxy Redshift Survey was undertaken using the Two-degree Field facility on the 3.9m Anglo-Australian Telescope.

The success of the survey was made possible by the dedicated efforts of the staff of the Anglo-Australian Observatory, both in creating the 2dF instrument and in supporting the survey observations.

Funding for the SDSS and SDSS-II has been provided by the Alfred P. Sloan Foundation, the Participating Institutions, the National Science Foundation, the U.S. Department of Energy, the National Aeronautics and Space Administration, the Japanese Monbukagakusho, the Max Planck Society, and the Higher Education Funding Council for England. The SDSS Web Site is <http://www.sdss.org/>.

The SDSS is managed by the Astrophysical Research Consortium for the Participating Institutions. The Participating Institutions are the American Museum of Natural History, Astrophysical Institute Potsdam, University of Basel, Cambridge University, Case Western Reserve University, University of Chicago, Drexel University, Fermilab, the Institute for Advanced Study, the Japan Participation Group, Johns Hopkins University, the Joint Institute for Nuclear Astrophysics, the Kavli Institute for Particle Astrophysics and Cosmology, the Korean Scientist Group, the Chinese Academy of Sciences (LAMOST), Los Alamos National Laboratory, the Max-Planck-Institute for Astronomy (MPIA), the Max-Planck-Institute for Astrophysics (MPA), New Mexico State University, Ohio State University, University of Pittsburgh, University of Portsmouth, Princeton University, the United States Naval Observatory, and the University of Washington.

## REFERENCES

- Adelman-McCarthy J., et al., 2006, *ApJS*, 162, 38  
 Angulo R.E., Baugh C.M., Frenk C.S., Lacey C.G., 2007, *MNRAS* submitted, astro-ph/0702543  
 Astier P., et al., 2006, *A&A*, 447, 31  
 Blanton M.R., Lin H., Lupton R.H., Maley F.M., Young N., Zehavi I., Loveday J., 2003, *AJ*, 125, 2276  
 Bond, J.R. & Efstathiou, G. 1984, *ApJ*, 285, L45  
 Bond, J.R., & Efstathiou, G., 1987, *MNRAS*, 226, 655  
 Blake C. & Glazebrook K., 2003, *ApJ*, 594, 665  
 Clarkson C., Cortes M., Bassett B.A., 2007, astro-ph/0702670  
 Cole S., et al., 2005, *MNRAS*, 362, 505  
 Coles P., Jones B., 1991, *MNRAS*, 248, 1  
 Colless M., et al., 2001, *MNRAS*, 328, 1039  
 Colless M., et al., 2003, astro-ph/0306581  
 Cooray A., Sheth R., 2002, *Physics Reports*, 372, 1  
 Crocce M., Scoccimarro R., 2007, PRD submitted, astro-ph/0704.2783  
 Eisenstein D.J., Hu W., 1998, *ApJ*, 496, 605  
 Eisenstein D.J., et al., 2001, *AJ*, 122, 2267  
 Eisenstein D.J., et al., 2005, *ApJ*, 633, 560  
 Eisenstein D.J., Seo H.-J., White M., 2007, *ApJ*, 664, 660  
 Feldman H.A., Kaiser N., Peacock J.A., 1994, *MNRAS*, 426, 23  
 Fukugita M., Ichikawa T., Gunn J.E., Doi M., Shimasaku K., Schneider D.P., 1996, *AJ*, 111, 1748  
 Górski, K.M., Hivon E., Banday A.J., Wandelt B.D., Hansen F.K., Reinecke M., Bartelmann M., 2005, *ApJ*, 622, 759  
 Gunn J.E., et al., 1998, *AJ*, 116, 3040  
 Gunn J.E., et al., 2006, *AJ*, 131, 2332  
 Hogg D.W., Finkbeiner D.P., Schlegel D.J., Gunn J.E., 2001, *AJ*, 122, 2129  
 Holtzman J.A. 1989, *ApJS*, 71, 1  
 Huetsi G., 2006, *A&A*, 449, 891  
 Ivezić Z., et al., 2004, *AN*, 325, 583  
 Lewis A., Challinor A., Lasenby A., 2000, *ApJ*, 538, 473  
 Meiksin A., White M. & Peacock J.A., 1999, *MNRAS*, 304, 851  
 Nichol R., 2007, ASP conference series (Proceedings of the "Cosmic Frontiers" conference, Durham, July 2006), astro-ph/0701073  
 Peacock J.A., Smith R.E., 2000, *MNRAS*, 318, 1144  
 Peebles, P. J. E. & Yu J. T., 1970, *ApJ*, 162, 815  
 Percival W.J., et al., 2001, *MNRAS*, 327, 1297  
 Percival W.J., Verde L., Peacock J.A., 2004, *MNRAS*, 347, 645  
 Percival W.J., et al., 2007a, *ApJ*, 657, 51  
 Percival W.J., et al., 2007b, *ApJ*, 657, 645  
 Pier J.R., Munn J.A., Hindsley R.B., Hennessy G.S., Kent S.M., Lupton R.H., Ivezić Z., 2003, *AJ*, 125, 1559  
 Press W.H., Teukolsky S.A., Vetterling W.T., Flannery B.P., 1992, *Numerical recipes in C. The art of scientific computing*, Second edition, Cambridge: University Press.  
 Riess A.G., et al., 2004, *ApJ*, 607, 665  
 Scherrer R.J., Weinberg D.H., 1998, *ApJ*, 504, 607  
 Seljak U., 2000, *MNRAS*, 318, 203  
 Seo H.-J., Eisenstein D.J., 2003, *ApJ*, 598, 720  
 Seo H.-J., Eisenstein D.J., 2005, *ApJ*, 633, 575  
 Seo H.-J., Eisenstein D.J., 2007, *ApJ*, 665, 14  
 Silk J., 1968, *ApJ*, 151, 459  
 Smith J.A., 2002, *AJ*, 123, 2121  
 Smith R.E., Scoccimarro R., Sheth R.K., 2007a, PRD, 75, 063512  
 Smith R.E., Scoccimarro R., Sheth R.K., 2007b, PRD submitted, astro-ph/0703620  
 Spergel D.N., et al., 2007, *ApJS*, 170, 377  
 Springel V., et al., 2005, *Nature*, 435, 629  
 Stoughton C., et al., 2002, *AJ*, 123, 485  
 Strauss M.A., et al., 2002, *AJ*, 124, 1810  
 Sunyaev, R.A., & Zel'dovich, Ya.B., 1970, *Astrophys. & Space Science*, 7, 3  
 Tegmark M., et al., 2006, PRD, 74, 123507  
 Tucker D.L., et al., 2006, *AN*, 327, 821  
 White M., 2005, *Astroparticlephys.*, 24, 334  
 Wild V., et al., 2005, *MNRAS*, 356, 247  
 York D.G., et al., 2000, *AJ*, 120, 1579

## APPENDIX A: LIKELIHOOD CALCULATION

The best fit parameters from our analysis of BAO are  $r_s/D_V(0.2) = 0.1980 \pm 0.0058$  and  $r_s/D_V(0.35) = 0.1094 \pm 0.0033$ , with correlation coefficient of 0.39. A multi-variate Gaussian likelihood can be estimated from using these numbers given model values of  $r_s/D_V(0.2)$  and  $r_s/D_V(0.35)$  as  $-2 \ln \mathcal{L} \propto \mathbf{X}^{-1} \mathbf{V}^{-1} \mathbf{X}$ , where

$$\mathbf{X} = \begin{pmatrix} \frac{r_s}{D_V(0.2)} - 0.1980 \\ \frac{r_s}{D_V(0.35)} - 0.1094 \end{pmatrix}, \quad (\text{A1})$$

$$\mathbf{V}^{-1} = \begin{pmatrix} 35059 & -24031 \\ -24031 & 108300 \end{pmatrix}. \quad (\text{A2})$$